minerals

MDPI

Article

Effect of a SO_2 Rich Atmosphere on Tempera Paint Mock-Ups. Part 1: Accelerated Aging of Smalt and Lapis Lazuli-Based Paints

José Santiago Pozo-Antonio [1,*], Teresa Rivas [1], Amelia Dionísio [2], Diana Barral [1] and Carolina Cardell [3]

1 Dpto. de Enxeñaría de Recursos Naturais e Medio Ambiente, Universidade de Enxeñaría de Minas e Enerxía, Universidade de Vigo, 36310 Vigo, Spain; trivas@uvigo.es (T.R.); dianabarral@uvigo.es (D.B.)
2 CERENA, Instituto Superior Técnico, Universidade de Lisboa. Av. Rovisco Pais, 1049-001 Lisboa, Portugal; amelia.dionisio@ist.utl.pt
3 Department of Mineralogy and Petrology, Faculty of Science, University of Granada, 18071 Granada, Spain; cardell@ugr.es
* Correspondence: ipozo@uvigo.es; Tel.: +34-986814077

Received: 16 March 2020; Accepted: 6 May 2020; Published: 10 May 2020

Abstract: The behavior of historic tempera paints exposed to pollutant gases is an important issue when developing conservation strategies. In this work, binary tempera paint mock-ups that were made with either smalt or lapis lazuli pigments mixed with either rabbit glue or egg yolk binders were exposed to an SO_2 accelerated aging test in order to find out more about the forms and mechanisms of alteration resulting from pigment-binder interaction. To this end, spectrophotometry, hyperspectral image analysis, and profilometry were used to study macro-scale, physical changes taking place on the surface of the paints, affecting color, gloss, reflectance, and roughness. Likewise, chemical and mineralogical changes were evaluated by X-ray diffraction (XRD), Fourier transform infrared spectroscopy (ATR-FTIR), polarized light microscopy (PLM), and scanning electron microscopy with micro-analysis (SEM-EDS), which was also used to visualize micro-texture changes in the paints. The smalt-based tempera showed a higher degree of deterioration than the lapis lazuli-based tempera, in particular a notable whitening related to the precipitation of sulfate-rich salts and to binder and pigment chemical alterations. Moreover, whereas aged egg yolk-based paints showed visible color change due to damage to the oily binder and the pigments, the most evident change in rabbit glue-based paints was binder loss. The alteration suffered by the pigments varied in line with their composition; thus, smalt (blue cobalt-containing glass) grains were more sensitive to SO_2 exposure than lapis lazuli-$(Na,Ca)_8[(S,Cl,SO_4,OH)_2|(Al_6Si_6O_{24})]$-crystals. In the smalt grains, the SO_2 test caused K^+ leaching from the glass matrix, which was detected by means of K/Co ratios, but the lazurite crystals (main component of lapis lazuli) were unaffected (regardless of the binder used in the tempera). The most likely source of the crystallized sulfate rich salts were the impurities that were detected in association with the natural lapis lazuli pigment, i.e., calcite and diopside. Indeed, the precipitation of efflorescences is the main cause of the optical changes found in the smalt- and lapis lazuli-based tempera, in addition to the physical-chemical damage to the binders. The information reported here would be useful for preventive conservation, as well as for art restorers, who are planning work on paintings in which paints of this kind were used.

Keywords: tempera paint; inorganic pigment; proteinaceous binder; sulfur dioxide; physical-chemical change; sulfate-rich salt; aging

1. Introduction

The SO_2 levels in some cities (e.g., in the Mediterranean area) still surpass the limits recommended by the World Health Organizations (WHO), despite the fact that SO_2 concentration in the atmosphere has been reduced in Europe in the last two decades due to European guidelines [1]. SO_2 can damage cultural heritage monuments and other works of art in polluted urban areas [2–7]. The role of the deposition and oxidation of SO_2 in the formation of gypsum ($CaSO_4{\cdot}2H_2O$) rich crusts on the surface of stones has been established in both sedimentary (carbonate) and silicate rocks [5–7]. On sedimentary carbonate stones, gypsum crusts form as a result of wet or dry deposition of SO_2 and the subsequent reaction of the sulfur with the calcium contained in the stone by means of various different processes ([8], and references therein). Gypsum-rich crusts have been studied on building materials that have been used in numerous cultural heritage monuments [9,10]. Sulfation mechanisms have also been described in decorative materials and mural paintings in a range of historical buildings, such as houses in Pompeii, which are exposed to medium/high SO_2 levels due to the site's proximity to Naples and to active volcanoes in southern Italy [2,3]. In "Villa Sora" (Torre del Greco near Pompeii), Cotte et al. [2] found that the lime-based mortar in the paintings had sulfated into gypsum and, in the Marcus Lucretius House, Maguregui et al. [3] identified the formation of gypsum from the lime-rich plaster, the transformation of red hematite into black magnetite, and the formation of Fe-rich sulfates on the wall paintings due to exposure to SO_2 in the atmosphere.

Although being a medium-sized, non-industrial city, Granada in southern Spain, which is well-known for the Alhambra (a UNESCO World Heritage site), is one of the most polluted cities in Western Europe [1], with annual mean concentrations of SO_2 and O_3 in excess of WHO recommendations (e.g., 11.85 $\mu g/m^3$ SO_2 in 2013) [11]. For this reason, over the last decade, several research projects (EXPOAIR and AERIMPACT, see acknowledgments) have been launched aimed at analyzing the impact of urban atmospheric aerosols on paints in open-air architectural monuments. As part of these investigations, long-term outdoor exposure tests and accelerated aging tests (ultraviolet irradiation—UV, temperature—T and relative humidity—RH cycling, and pollutant gases) were performed while using tempera paint mock-ups. Mixing an inorganic pigment with a water-soluble proteinaceous binder, e.g., egg yolk or rabbit glue, is utilized to produce traditional tempera [12]. The mock-ups used in these projects were binary mixtures of either egg yolk or rabbit glue with a mineral pigment. Lapis lazuli and blue smalt were the pigments selected for testing, since they have been important in historical paintings and, likewise, have been identified in Granada polychromed decoration [13–16]. In particular, lapis lazuli of different quality has been found in paintings from the Alhambra palaces [13–16]. Here, there is no scientific evidence of sulfation on the so-far studied decorative paintings, despite the high SO_2 atmospheric levels reported in the city [11]. Instead, chloride-induced degradation was recognized through the identification of mixed-cation chloride compounds in synthetic red lead (Pb_3O_4), cinnabar (HgS), azurite ($Cu_3(CO_3)_2(OH)_2$), and malachite ($Cu_2CO_3(OH)_2$) pigments. Chemical degradation was also observed in gilded tin decoration, while the best preserved of all the pigments in the polychromes at the Alhambra palaces are lapis lazuli and ultramarine, showing their high resistance to weathering [13,16]. The identification of diopside ($CaMgSi_2O_6$), a common mineral that is related with lapis lazuli in nature, made it possible to discern between the natural or synthetic origins of these blue pigments in the Alhambra paintings. Moreover, the Raman spectrum of the lapis lazuli pigments indicated their provenance from the Badakhshan region of Afghanistan [17].

Egg yolk is composed of (58%) fatty acids (oleic and linoleic acids as unsaturated fatty acids and palmitic and stearic acids as saturated fatty acids) and (32%) proteins [18]. Rabbit glue is mainly composed of collagen [19]. In addition to the characteristics of the mineral/inorganic pigment, the type and amount of binder, which can affect the color, superficial roughness, consistency, and weathering behavior of the paint, also directly influences the final appearance of the tempera paint [12,20–22]. In principle, egg yolk, which dries faster than rabbit glue, is longer lasting and makes the paint brighter and more flexible [12,20]. The components of the tempera paint (binder and pigment) must be blended in precise proportions to achieve a smooth-spreading paint layer, which must also be

consistent. The precise amount of binder to be mixed with a particular pigment (which also affects the surface properties of the paint) depends on the nature of the pigment and its grain size [12,23,24]. Generally, the smaller the pigment particle size, the higher the amount of binder that needs to be added [22,23]. The pigment particle size affects the color and the hiding power of the paint, and also plays a key role in the optical appearance and surface finish of the paint layer [22,25]. Recent research studies have pointed out that impurities present in historical pigments could significantly alter the optical, chemical, and physical properties of the whole paint system, in that they can influence pigment-binder interaction and, thus, the aging behavior of the paint [22,26,27].

In the last two decades, research conducted on historical paints using mock-ups has increased in order to fully characterize the mineralogical and physical changes affecting oil/tempera paints that were subjected to exposure to the natural environment or artificial accelerated tests [11,21,28–36]. The weathering mechanisms taking place in these paints have been related to (i) the type and amount of binder, (ii) the nature of the mineral pigment (chemical composition, impurities, and neoformed minerals), and (iii) the pigment-binder interaction [21,23,27,30–36]. As mentioned, the response of a paint to aging varies according to the type of binder that it contains [21]. Rivas et al. [21] found that, with exceptions, egg yolk-based paint mock-ups made with one of the following pigments: chalk ($CaCO_3$), gypsum ($CaSO_4{\cdot}2H_2O$), white lead ($PbCO_3/Pb_3(CO_3)_2(OH)_2$), hematite ($Fe_2O_3$), cinnabar (HgS), azurite ($Cu_3(CO_3)_2(OH)_2$), and lapis lazuli ($(Na,Ca)_8[(S,Cl,SO_4,OH)_2|(Al_6Si_6O_{24})]$) with different grain sizes and subjected to a real marine and industrial environment, were more resistant to decay than equivalent paints that were prepared with rabbit glue binder, when subjected to outdoor (natural) marine and industrial exposure [21]. Elert and Cardell found significant conformational changes in the egg yolk binder while working with cinnabar-based tempera mock-ups with egg yolk binder exposed to UV- and sunlight-based tests [24]. In other research based on calcium sulfate-based paints mock-ups with rabbit glue exposed to high RH and to water spray tests, the authors recommended the use of a more water resistant material than animal glue, such as casein or egg yolk, because they found, in the rabbit glue-based paints, that volumetric changes due to the mineralogical transformation could accelerate paint loss [35].

Having verified sulfation in lime-based paints that were prepared with either egg yolk or rabbit glue [11], the SO_2 effect on tempera mock-ups made with mixtures of these binders with other inorganic pigments should be investigated in order to improve our knowledge of the weathering mechanisms affecting paints. This can then be applied in the preventive conservation of historical paintings and can help to ensure longer-lasting restorations. To this end, we conducted an in-depth study on the effect of SO_2 on blue and green tempera mock-ups made with one of the following pigments: smalt (blue cobalt-containing glass), lapis lazuli ($(Na,Ca)_8[(S,Cl,SO_4,OH)_2|(Al_6Si_6O_{24})]$), azurite ($Cu_3(CO_3)_2(OH)_2$), and malachite ($Cu_2CO_3(OH)_2$) pigments mixed with either rabbit glue or egg yolk as binders. This was done using an accelerated SO_2 aging test while using a climatic chamber in *Instituto Superior Tecnico* (University of Lisbon, Portugal). In this paper, which is Part 1 of a series entitled *Effect of a SO_2 rich atmosphere on tempera paint mock-ups*, we present and discuss the results that were obtained due to SO_2 exposure of smalt- and lapis lazuli–based tempera paints. In a second article (Part 2), also published in this Special Issue of *Historical Mineral Pigments*, we show the results of research into the impact of SO_2 on azurite (different grain sizes) and malachite-based tempera paints.

Blue smalt is a synthetic potash silicate pigment made by mixing cobalt (Co) oxide (cobalt-potassium silicate glass) with molten glass [36], which itself is made from three main materials, i.e., sand (SiO_2), limestone ($CaCO_3$), and sodium carbonate (Na_2CO_3). This pigment does not have a precise chemical formula and its composition can vary, as follows: cobalt oxide = 2–18%, silica = 66–72%, and potassium in the form of potassium carbonate (10% to 21%), which is added to the glass to act as a flux. It might also contain impurities, such as oxides of copper (Cu), magnesium (Mg), sodium (Na), nickel (Ni), manganese (Mn), and barium (Ba). Once the glass melts, the glass is exposed to cold water to create a thermal shock, which breaks the glass into several chunks. These pieces of glass are then ground into a fine powder. Its use features in paintings back to 11th and 12th century wall paintings in Mongolia and Turkey [37]. It appeared

in Europe at the beginning of the 15th century and it was largely used in important Italian artistic contexts such as Rome and Florence at the end of this century. It became a substitute for azurite and lapis lazuli in the 17th century [38], perhaps because it was cheaper than other blue pigments, such as azurite [39]. In decorated stained glass, a layer of smalt mixed with a binding agent (gum arabic or an essential oil) is deposited on the glass and then exposed to 600–700 °C [36]. The discoloration (fading) of blue smalt-based paints was attributed to the leaching of potassium (K^+) ions from the glass matrix towards the binding medium, causing an increase in pH and the subsequent rearrangement of the structure, specifically a change in the cobalt coordination from tetrahedral to octahedral [36,40,41]. Robinet et al. showed that this process causes an increase in the Co-O distance in the altered pigment [42]. These authors [42] also stated that the alteration in the color of smalt that was caused by this process resulted in a change in the K/Co ratio: a K/Co ratio of 1/1 or higher corresponds to non-altered smalt, whereas K/Co ratios of less than 1 are typical of faded smalt grains. Spring et al. [43] found that the K^+ leached from the glass can form potassium soaps on the surfaces, inducing a darkening of the organic medium and, subsequently, a grey-brown appearance of the paint. For other authors [44], smalt deterioration occurs through various combined processes, both physical, such as the formation of a crack network due to hydration of the glass, and chemical, e.g., leaching of cobalt ions, which leads to pigment discoloration, darkening of the oil medium due to alkaline loss from the glass, or K/Co soap and salt formation (in oil-rich paints).

Lapis lazuli was one of the most used mineral pigments in medieval tempera paints. It is a natural pigment that is obtained by grinding the semi-precious stone lapis lazuli, whose main component is lazurite. Lazurite is a tectosilicate -($Na_6Ca_2(Al_6Si_6O_{24})(SO_4,S,S_2,S_3,Cl,OH)_2$)- belonging to the sodalite group, which is formed through contact metamorphism of limestones and is naturally associated with diopside ($CaMgSi_2O_6$), forsterite (Mg_2SiO_4), wollastonite ($CaSiO_3$), calcite ($CaCO_3$), and pyrite (FeS_2). Lapis lazuli was a very expensive pigment, so that it was often mixed with cheaper blue pigments, such as azurite and indigo (natural blue dye) [45]. Lapis lazuli has been widely used since ancient times—there is evidence of its use in cave paintings in Afghan temples from the 6th and 7th centuries AD—although it was most extensively used in the 14th and 15th centuries, in illuminated manuscripts, Italian panel paintings, and even in mural paintings [45,46]. Lapis lazuli was also used in the paintings that cover the *yeserías* (plasterwork) and woodwork decoration in the Alhambra palaces (Granada, Spain) [13,14].

In this research paper (Part 1 of the series entitled *Effect of a SO_2 rich atmosphere on tempera paint mock-ups*) smalt- and lapis lazuli-based tempera paint mock-ups that were prepared with different binders—i.e., egg yolk or rabbit glue—were subjected to an SO_2 aging test, and their behavior was evaluated in terms of compositional (chemical and mineralogical) and physical changes as a result of pigment-binder interactions.

2. Materials and Methods

2.1. Tempera Paint Mock-Ups

In this study, we used six tempera paint mock-ups that were prepared as binary mixtures (inorganic pigment and organic binder) that mimicked real tempera paints. Two organic binders were selected: egg yolk (albumin, ovalbumin, and fatty acids), named E hereafter, obtained from locally purchased eggs, and rabbit glue (collagen pearls, ref. 63028) named R hereafter, that was supplied by *Kremer* Pigments GmbH & Co (Aichstetten, Germany). The inorganic pigments selected for this study were lapis lazuli (LAP hereafter) and smalt (SM hereafter), both of which were supplied by *Kremer* Pigments GmbH & Co. KG (Aichstetten, Germany). Two different grain sizes (coarse-C and extra-coarse-EC, see Table 1) were selected for the SM pigment in order to identify the influence of grain size on the durability of the paints against SO_2 exposition.

Table 1. Mineralogical/Chemical composition and grain size of the pigments according to *Kremer* supplier and to the authors [22], binder (egg yolk and rabbit glue) content in the tempera mock-ups, and mineral phases identified in the tempera mock-ups by XRD before and after SO_2 exposure. The author references are also shown. E-T: egg yolk-based temperas and R-T: rabbit glue-based temperas. Mm: maximum grain size and *r*: grain size range.

Kremer Reference	Authors Reference	Kremer Composition	Authors Composition [22]	Kremer PigmentSize (μm)	Authors Particle Size (μm) [22]	Paint's Binder Content (%) [22]		Authors Composition before SO_2		Authors Composition after SO_2	
						E-T	R-T	E-T	R-T	E-T	R-T
Lapis lazuli No. 10540, crystalline (natural pale)	LAP	Haüynite	Lazurite Calcite Diopside	< 80	Mm = 47 *r* = 0.6–95	27	18	Lazurite Calcite Diopside	Lazurite Calcite Diopside	Lazurite Calcite Diopside Gypsum Bassanite Pentahydrite	Lazurite Calcite Diopside Gypsum Bassanite Pentahydrite
Smalt coarse No. K10010	SM-C (coarse)	Blue glass, Co-silicate	n.d.	80	Mm = 55 *r* = 1–100	43	21	n.d.	n.d.	Thenardite	Aphthitalite
Smalt standard No. K10000	SM-EC (extra coarse)	Blue glass, Co-silicate	n.d.	0–120	Mm = 75 *r* = 1–140	37	20	n.d.	n.d.	Thenardite	n.d.

LAP: lapis lazuli; SM: smalt; C: coarse grain size; EC: extra coarse grain size; Mm: maximum grain size; R: grain size range; n.d. not detected; Haüynite: $(Si_3Al_3)Na_3CaO_{12}S$; Lazurite: $Na_6Ca_2(Al_6Si_6O_{24})(SO_4,S,S_2,S_3,Cl,OH)_2$-; Calcite: $CaCO_3$; Diopside: $MgCaSi_2O_6$; Gypsum. $CaSO_4{\cdot}2H_2O$; Bassanite: $CaSO_4{\cdot}1/2H_2O$; Pentahydrite: $MgSO_4{\cdot}0.5H_2O$; Thenardite: Na_2SO_4; Aphthitalite: $K_3Na\ (SO_4)_2$.

The paint mock-ups were prepared by mixing one proteinaceous binder with one pigment according to the recipes of the Old Masters in order to achieve standards that are similar to those used by medieval artists [47]. The procedure for making the E-based paints can be consulted in [33], and for the R-based paints in [23]. These paints contain varying amounts of organic binder, because binder demand depends on the chemical composition and particle size of the pigment (Table 1). For the E-based paints, ca. 0.5 g of each powdered pigment was placed in a small bowl and different amounts of beaten egg yolk were added to form a fluid paste. For the R-based paints, the rabbit glue pearls (8 g) were previously soaked in 100 mL deionized water for 24 h under stirring before heating below 50 °C in a water bath until a homogeneous mixture was obtained. In order to prepare a tempera paint of appropriate consistency, 0.5 g of each pigment was first wetted with deionized water and mixed afterwards with sufficient animal glue paste.

The binary paints that were obtained were then painted onto glass slides (ca. 76 mm × 26 mm × 1 mm) while using a paintbrush. Several layers were applied (once the previous layer was completely dry) in order to properly cover the substrate. The paint mock-ups were labeled using the acronym of the pigment, LAP for lapis lazuli, and SM for smalt, followed by the grain size, i.e., coarse -C- and extra-coarse -EC-, and finally, the letter E to refer to egg yolk or the letter R for rabbit glue (see Table 1).

Additional mock-ups were prepared with each binder by itself for comparison purposes (Figure 1). These were prepared by painting the binder onto a glass slide using a paintbrush. Subsequently, all of the paint mock-ups were kept under laboratory-controlled conditions (18 ± 5 °C; 60 ± 10% RH) for one month, in which they were protected from light exposure. Subsequently, each tempera paint and solely binder mock-up was cut into two pieces (so creating two paint samples of 38 mm × 26 mm × 1 mm); the fresh reference sample was kept under the aforementioned storage conditions, and the other sample was subjected to the SO_2 test.

2.2. SO_2 Accelerated Aging Test

The tempera mock-ups and the binder mock-ups were placed in a FITOCLIMA 300EDTU climatic chamber (25 °C; 45% RH) in the *Instituto Superior Tecnico* in Lisbon (Portugal), where they were exposed to SO_2 gas for two months. The SO_2 was diluted at 3% in 3000 ppm of nitrogen and then dosed at a concentration of 200 ppm, a value more than 250,000 times higher than current SO_2 levels in most of Europe (average value 0.00076 ppm) [48]. The reference fresh samples were stored under laboratory-controlled conditions (18 ± 5 °C; 60 ± 10% RH) and light-protected during these two months.

The tap water used in the chamber to produce the RH (45%) was analyzed by high-resolution liquid chromatography (HRLC) (Metrohm instrument with Metrosep A Supp5–250 column, Metrohm, Herisau, Switzerland) and Inductively Coupled Plasma-Optical Emission Spectroscopy (ICP-OES) (Perkin Elmer Optima 4300 DV ICP-EPS, PerkinElmer, Waltham, MA, USA) providing the following composition: 15.8 mg/L Cl^-, <0.05 mg/L $NO_2{}^-$, 2.15 mg/L $NO_3{}^-$, 23.7 mg/L $SO_4{}^{2-}$, 0.017 mg/L Ba^{2+}, 17.35 mg/L Ca^{2+}, 2.37 mg/L K^+, 3.74 mg/L Mg^{2+}, and 13.18 mg/L Na^+.

2.3. Analytical Methods

The reference (fresh) and SO_2 aged paint and binder mock-ups were characterized while using the following techniques:

The mineralogical composition (when possible) was obtained using X-ray diffraction (XRD) via a Siemens D5000 (Siemens, Munich, Germany), by applying the random distribution of powder particles. Analyses were performed using Cu-Kα radiation, Ni filter, 45 kV voltage, and 40 mA intensity. The exploration range was 3° to 60° 2θ and the goniometer speed was 0.05° 2θ s^{-1}. The identification of each mineral phase was determined using the X'Pert HighScore (Malvern Panalytical B.V., Almelo, The Netherlands).

A stereomicroscope (SMZ 1000, Nikon, Brighton, MI, USA) was used to examine the textural and chromatic features of the surfaces of the mock-ups.

The color changes in the tempera paints and the binder mock-ups were characterized using CIELAB color space [49,50] measuring L* (lightness), a* and b* (color coordinates) using a Minolta CM-700d spectrophotometer (Minolta, Osaka, Japan). L* is the lightness ranging from 0 (absolute black) to 100 (absolute white); a* indicates the color position between red (positive values) and green (negative values) and b* between yellow (positive values) and blue (negative values). Nine measurements were randomly taken for each sample to provide statistically consistent results. The measurements were made in the Specular Component Included (SCI) mode, for a spot diameter of 3 mm, while using D65 as the illuminant and an observer angle of 10°. Color data were processed as color differences (ΔL*, Δa* and Δb *) and global color change (ΔE^*_{ab}) between the initial color and that of the aged surface in order to evaluate the color changes [49,50]. Therefore, the higher the value, the more visible the color change. A global color change (ΔE^*_{ab}) of more than 3.5 CIELAB units represents a color change visible to a non-expert observer [51].

The gloss value (G), which is the amount of specularly reflected light when compared to the amount of diffusely reflected light, and its variation (ΔG) were obtained by means of a Konica Minolta Unigloss 60Plus (Konica Minolta, Kyoto, Japan). A reflection angle of 60° was used and three measurements were taken per sample.

A profilometer Mitutoyo SJ400 (Mitutoyo, Takatsuku, Kawasaki, Kanagawa, Japan) characterized roughness to assess the relief of the samples before and after exposure to SO_2 through the arithmetic average roughness (Ra, μm), root mean square roughness (Rq, μm), and average maximum profile height (Rz, μm) described in [52]. The equipment traced a scan length of 2 cm, and three profiles per sample were obtained.

The change in reflectance in each aged paint and binder mock-up was obtained while using a hyperspectral camera. The equipment consisted of a CCD sensor Pulnix TM-1327 GE (1040 rows, 1392 columns, PULNiX America Inc., California, United States), with an objective lens with a focal length of 10 mm. An ImSpector V10 spectrograph with a spectral range of 400–1000 nm and a spectral resolution of 4.55 nm was positioned between the sensor and the lens. The spectral camera recorded a linear array of 1392 pixels at 1040 wavelengths in the range 400–1000 nm. The camera scans the surface line-by-line in order to obtain an image at each of the 1040 wavelengths. A Schott DCR® III incandescent lamp (SCHOTT-FOSTEC, LLC, New York, United States) with a rectangular head of 51 mm long and 0.89 mm wide was used as a light source. A cylindrical lens placed in front of the lamp that was focused the light to produce an illuminated area that was 15 cm long and 1 cm wide. The sample was placed on a motorized XYZ translation stage in which the Z- axis was perpendicular to the sample surface. The paint mock-ups were fully scanned. Once the hyperspectral images were acquired, the data were processed in a MATLAB programming environment in order to display the respective reflectance graphs.

Molecular composition was obtained by Attenuated Transmittance Reflectance–Fourier transform infrared spectroscopy (ATR-FTIR) with a Thermo Nicolet 6700 (Thermo Fisher Scientific, Waltham, MA, USA). The infrared (IR) spectra were recorded at 2 cm^{-1} resolution over 100 scans from 400 to 4000 cm^{-1}.

A sample ca. 4 mm × 26 mm × 1 mm was cut from the glass slides of each paint sample (fresh and aged samples), embedded in styrene resin, and then cut in order to obtain a cross section with which to study in-depth the alterations in the tempera paints from the exposed surface toward their interior. Thus, cross-sections that were prepared as thin sections were visualized with an Axioscope 5 (Zeiss, Oberkochen, Germany) polarized light microscope (PLM).

The micromorphological and chemical characterization of all paint mock-ups was obtained using a scanning electron microscope (SEM) with energy-dispersive X-ray spectroscopy (EDS) (Philips XL30-Philips, Amsterdam, Netherlands and FEI Quanta 200- Thermo Fisher Scientific, Waltham, MA, USA) in both Secondary Electron (SE) and Back Scattered Electron (BSE) modes. Both the carbon-sputtered chip surfaces and the cross sections were studied. Optimum observation conditions

were obtained at an accelerating potential of 15–20 kV, a working distance of 9–11 mm, and specimen current of 60 mA. The acquisition time for recording EDS spectra, i.e., the dwell time, was 40–60 s.

The static contact of the fresh paint and binder mock-ups was measured while using a goniometer SEO Phoenix-300 Touch (Kromtek Sdn Bhd, Selangor D.E., Malaysia) following [53] and applying the sessile drop method (three drops of 6 μL of deionized water per sample).

3. Results and Discussion

Table 1 shows the mineralogical/chemical composition and grain size of the commercial pigments, as detailed by the supplier (*Kremer* Pigments GmbH & Co), plus those that were obtained by the authors using XRD during this and previous research [22]. Note that the information that was provided by *Kremer* did not fully coincide with the composition identified by the authors, as also reported for other pigments in previous works [22,23,35]. The authors found that the LAP pigment was composed of lazurite, calcite, and diopside, proving that this is a natural pigment (unlike the synthetic impurity-free ultramarine), while that reported by the manufacturer was haüynite, also known as haüyne, with empirical formula $Na_4Ca_2Al_6Si_6O_{22}S_2(SO_4)Cl_{0.5}$. Lazurite and haüyne are both cubic mineral varieties from the sodalite group (a member of the feldspathoids group), together with sodalite ($Na_8(Al_6Si_6O_{24})Cl_2$) and nosean ($Na_8(Al_6Si_6O_{24})(SO_4)H_2O$). Lazurite is the blue variety and the primary constituent of lapis lazuli, while haüyne varies in color from white or gray to green or blue. Members of the sodalite group often occur in the same rock together with amphiboles, olivine, pyroxenes, calcite, and/or pyrite, as mentioned earlier.

After exposure to SO_2, the formation of various neoformed mineral phases in the LAP mock-ups (irrespective of the binder present) were confirmed using XRD, in addition to those found in the LAP pigment, as shown in Table 1. The new phases included gypsum ($CaSO_4{\cdot}2H_2O$), bassanite ($CaSO_4{\cdot}1/2H_2O$) and pentahydrite ($MgSO_4{\cdot}0.5H_2O$), all of which are sulfate-based (Table 1). Natural lapis lazuli is not a pure mineral; it is a rock made of varied minerals (e.g., calcite, dolomite, pyrite, mica, diopside, albite, sodalite, etc.), each of one with different properties and therefore different susceptibility to weathering [54,55]. The impurities that are present in our LAP pigment are calcite and diopside. Following several works, these minerals are prone to dissolving under acidic, neutral, and basic pH conditions, releasing Ca, Si, and Mg cations to the media [55,56]. Accordingly, it is reasonable to suggest that the sulfate salts detected after this SO_2 test were precipitated due to the interaction of the LAP pigment grains with SO_2. Consequently, it is likely that pentahydrite was formed at the expense of diopside and the Ca-sulfate salts at the expense of calcite. As these two minerals are present in the LAP pigment in trace amounts, the confirmation that they have been altered to form neo-formed phases through the estimation of their content by means of XRD is, however, difficult. Mg and Ca, which make up these sulfates, could also come from the water used for the test. Nevertheless, this possibility is unlikely in the case of magnesium salt, because the Mg^{2+} content in the water was fairly low (see Section 2.2).

Various different sulfates were also detected in the SM mock-ups, such as thenardite (Na_2SO_4) in the SM-E-based paints (SM-C-E and SM-EC-E) and aphthitalite ($K_3Na(SO_4)_2$) in the R-based paint SM-C-R. No neoformed minerals were detected with XRD in the aged SM-EC-R. Smalt is a synthetic pigment that is made by mixing cobalt oxide with molten glass from sand (SiO_2), limestone ($CaCO_3$) and sodium carbonate (Na_2CO_3). Therefore, it could be that the interaction of the SO_2 with the SM pigments results in the formation of new Na/K-rich minerals. Potassium and sodium (chemically very similar) are strongly alkaline and their presence in the SM pigment assures the necessary level of alkalinity to maintain the SM's blue color. The acidic pH of the SO_2 deposition and oxidation process could favor the chemical degradation of the smalt pigment in SM paints.

The formation of the sulfated salts on the SM mock-ups could have been favored by the use of non-ultrapure water in the test, as was commented in the LAP paints. Nonetheless, the contribution of the water in the formation of aphthitalite ($K_3Na\ (SO_4)_2$) would be ruled out, since the content of K^+ in the water is really very low. On the one hand, the use of non-deionized water in this test has undoubtedly incorporated a variable that is difficult to control and it leads to more difficult

interpretation of the results of the tests; however, on the other hand, the studied system is more closely adjusted to the real exposure environment and, in this sense, the obtained results better reflect the pigments susceptibility to this type of aging.

Figure 1 shows stereomicroscope micrographs of the surfaces of the paint and binder mock-ups before and after the SO_2 test. As regards the binder mock-ups, the E-mock-up, before the test, has a cracked appearance and a yellowish tone, while the R-mock-up showed a continuous grayish color. After the SO_2 test, both of the binders reacted in a different way: in E-mock-up, the cracking phenomenon became more severe, whereas R-mock-up became more friable, resulting in a partial loss due to peel off the glass slide.

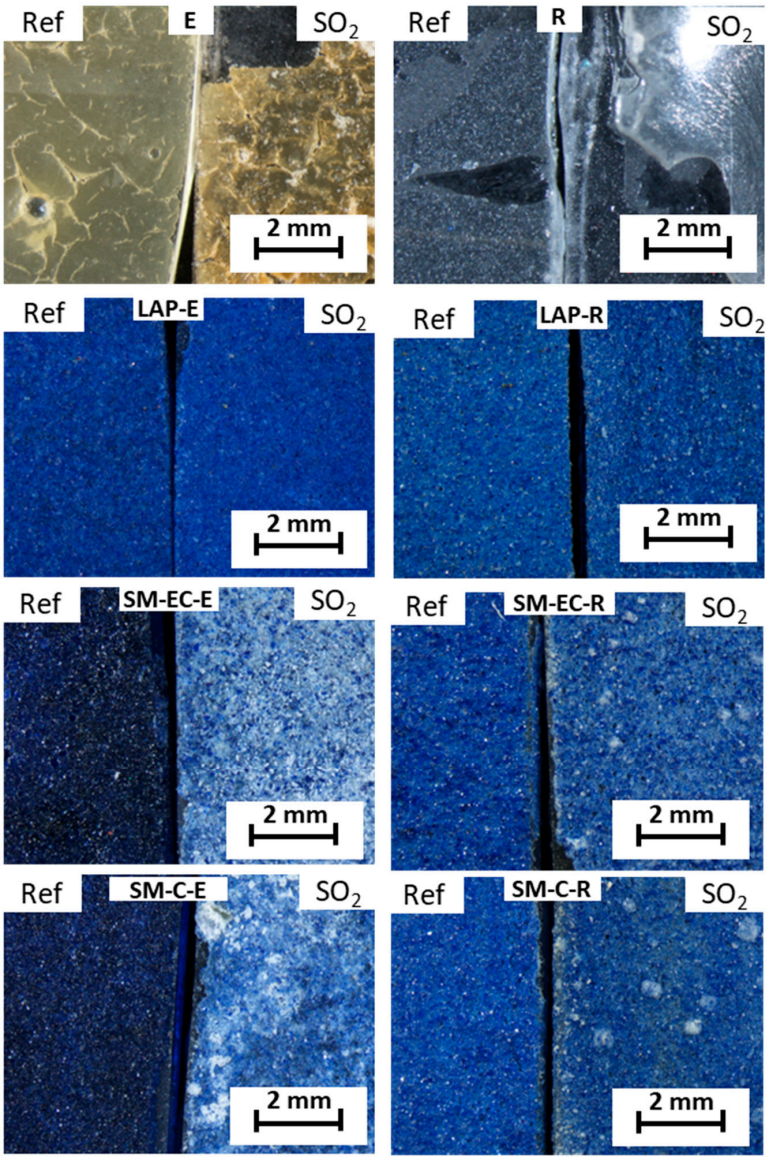

Figure 1. Micrographs taken with stereomicroscopy of the binders (E and R) and the tempera paint mock-ups made with either LAP or SM mixed with E or R. Note: Ref: reference sample; SO_2: SO_2 aged paints; C: coarse grain size; EC: extra-coarse grain size. Check Table 1 to better follow the paints labeling.

As regards the tempera mock-ups, the color of fresh SM-paints varied depending on the binder and the pigment grain size, in that the blue color was more intense in the E-paints when compared to those made with R (Figure 1). This intense blue color was particularly evident in the SM-paints and less so in the LAP-paints.

After SO_2 exposure, no visible color changes were detected on the LAP-paints after SO_2 exposure. Conversely, SM-paints acquired a visible whitish tone, especially those that were made with egg yolk (SM-EC-E, SM-C-E) (Figure 1). This whitening could be related to the precipitation on the surface of the different identified salts by XRD. Note that the discoloring of the surfaces of the SM-R-paints (SM-EC-R and SM-C-R) did not affect the entire surface, but was distributed in the form of spots; conversely, in SM-E-mock-ups, discoloration affected almost the entire surfaces, being much more intense. The different degree of discoloration that was exhibited by SM-E paint and SM-R paint could be due to a different amount of sulfated salts precipitated on the surfaces. However, it cannot be ruled out that the discoloration is due to deterioration of the smalt itself or even to a different interaction between the pigment and the binders. Indeed, it is known that smalt often discolors from blue to grayish when the pigment is present in an oily medium, such as egg yolk [40]; following these authors, this phenomenon is due to a reaction between the fatty acids (even in low proportions) and K. Hence, the presence of egg yolk (which is barely acidic to neutral, with pH ca. 6.5–6.7, [57]) might induce a slightly acidic environment in the SM paints that triggers the destabilization of K in the structure of the SM pigment.

Color spectrophotometry (Figure 2) confirmed the stereomicroscopy observations by revealing that, in all the paints, except for LAP-E, the L* coordinate was the color parameter that was most affected by SO_2 exposure. Thus, after SO_2 exposure, L* increased in the SM-mock-ups (regardless of the binder used) in line with the whiteness that was observed under stereomicroscopy. Conversely, L* decreased in the aged LAP-R-paint. In aged LAP-E paint, the most affected parameter was b*, which decreased (there was an increase in the bluish tone of the paint). However, in the SM-paints, the increase in b* suggests a shift towards yellow tones. It is important to highlight that, in the mock-ups made solely with binders, b* was also the most affected color parameter. However, the trend in b* was different for each binder: in the egg yolk, b* increased with a yellowing effect, while b* fell in the rabbit glue, denoting a loss of yellow tone (as seen in Figure 1). Coordinate a* increased in aged LAP-paints, regardless of the binder used (color became redder), while, in aged SM-paints, the a* value fell (they became greener).

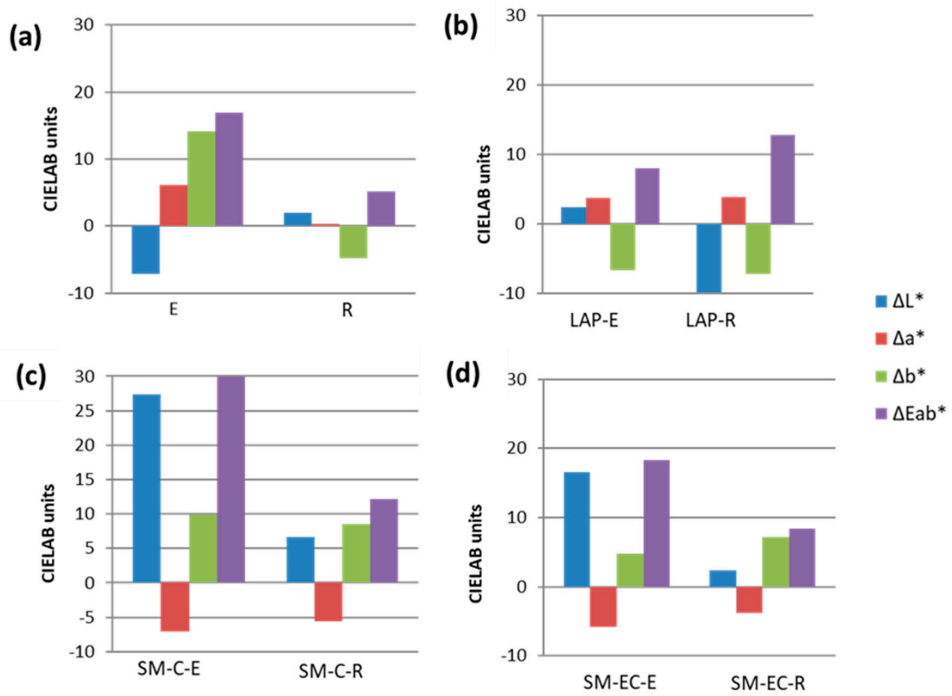

Figure 2. Variations in the color parameters (ΔL*, Δa*, Δb*, and ΔE^*_{ab}) of the paint and binder mock-ups after SO_2 exposure. (**a**) Binder (E and R) mock-ups. (**b**) Lapis lazuli (LAP) mock-ups. (**c**) Smalt (SM) mock-ups with a coarse (C) grain size. (**d**) Smalt (SM) mock-ups with an extra-coarse (EC) grain size. Check Table 1 to better follow the paints labeling.

The changes in color suffered after aging by all tempera mock-ups, as well as the binder mock-ups, were visible to the naked eye, as, in all cases, the global color changes (ΔE^*_{ab}) were higher than 3.5 CIELAB units [51]. SM-C-E paint showed the highest ΔE^*_{ab} (29.9 CIELAB units), while the LAP-E paint showed the lowest ΔE^*_{ab} (7.97 CIELAB units). The extent of the color change varied between LAP- and SM-paints. In LAP-paints, ΔE^*_{ab} was higher in R-based mock-ups, whereas, in SM paints, ΔE^*_{ab} was higher in the E-based mock-ups. In the latter, the paint prepared with the coarse pigment (SM-C-E) had a higher ΔE^*_{ab} value than the paint made with the extra-coarse pigment (SM-EC-E).

Regarding gloss, measurements on the reference (fresh) paints (Table 2) allowed us to confirm higher gloss values for binder mock-ups when compared to the values for tempera paint mock-ups; no statistically significant differences were found between the two binders (E and R). As regards the tempera mock-ups, those containing E had higher gloss values than their counterparts that were made with R. This trend was also detected in SO_2 aged paints. No relation was found between the grain size of pigments and the gloss value in the SM-paints (made with either coarse or extra-coarse SM). In general, the mock-ups showed negligible variations in gloss (Table 2), except for those that were prepared with just the binder. The sharp increase in the gloss value detected on the (solely binder) R-mock-up (27.27 ± 1.07 gloss units) is worthy of note; this increase could be due to the fact that the measurement was taken on the glass slide substrate, since, as observed with stereomicroscopy, almost all of the rabbit glue binder film had been lost after the SO_2 test. In the tempera mock-ups, the variation in the gloss value was less than one gloss unit. The highest gloss change was detected in LAP-E (−0.37 ± 0.06 gloss units) and the lowest in SM-C-R (0.01 ± 0.00 gloss units).

Table 2. Gloss values (G, gloss units), gloss variations (ΔG, gloss units), average maximum profile height (Rz, μm), and respective variation (ΔRz, μm) of paint and binder mock-ups before (before SO_2) and after (after SO_2) SO_2 exposure, while considering the fresh samples as a reference. Standard deviations are also shown. Check Table 1 to better follow the paints labeling.

Sample	$G_{\text{before SO2}}$	$G_{\text{after SO2}}$	ΔG	$Rz_{\text{before SO2}}$	$Rz_{\text{after SO2}}$	ΔRz(μm)
E	8.33 ± 0.06	4.67 ± 0.06	−3.67± 0.50	65.70 ± 10.66	191.57 ± 30.56	125.87 ± 32.37
R	7.50 ± 1.07	34.77 ± 1.07	27.27 ± 1.07	21.90 ± 29.13	150.80 ± 33.07	128.90 ± 44.07
LAP-E	1.30 ± 0.00	0.93 ± 0.06	−0.37 ± 0.06	45.17 ± 3.20	50.80 ± 4.69	5.63 ± 5.68
LAP-R	0.57 ± 0.06	0.40 ± 0.00	−0.17 ± 0.06	68.57 ± 3.59	68.00 ± 6.43	−0.57 ± 7.36
SM-C-E	1.10 ± 0.00	0.90 ± 0.00	−0.20 ± 0.00	62.77 ± 8.13	65.83 ± 11.07	3.07 ± 21.24
SM-C-R	0.59 ± 00	0.60 ± 0.00	0.01 ± 0.00	80.50 ± 4.81	89.56 ± 10.65	9.06 ± 11.69
SM-EC-E	1.10 ± 0.00	0.90 ± 0.00	−0.10 ± 0.00	116.73 ± 16.45	105.17 ± 35.02	−11.57 ± 38.69
SM-EC-R	0.80 ± 0.00	0.63 ± 0.06	−0.17 ± 0.06	100.80 ± 22.68	96.40 ± 11.45	−4.40 ± 25.41

Among all of the measured roughness parameters, the one that showed the greatest variation after the SO_2 test was Rz (average maximum profile height); for this reason, only this parameter, among the roughness parameter evaluated, will be discussed. Regarding fresh binder mock-ups (E and R), it can be seen that E-mock-up had a higher Rz than the R-mock-up. As regards the tempera paint mock-ups, we found that the R-based paints showed higher Rz values than the E-based paints, except for SM-C. However, it is important to note that in the SM-C-E and SM-C-R paints, the standard deviations of the measurements are greater than in the rest of the paints, which means that the differences cannot be considered to be statistically significant. The fresh paint mock-ups with the highest roughness values were those that were made with SM-EC pigment, followed by the SM-C-paints. This suggests that the higher the grain size, the higher the Rz value.

After the SO_2 aging test, the greatest change (increase) in Rz was observed in the binder (E and R) mock-ups. Surprisingly, there was an increase in roughness values in both SM-C paints made with either E or R, while, in both SM-EC paints these values fell. LAP–E paint showed an increase in roughness whereas in LAP-R paint there was a slight decrease. The highest decrease in roughness was found in the SM-C-E paint and the lowest increase was in LAP-R paint. Note that, although the

variations in roughness were not statistically significant, the values shown here can be used to compare the different paint mock-ups.

All of the paint mock-ups showed changes in their reflectance values after being exposed to SO_2 (Figure 3). However, these changes varied from one paint to the other, as was also noticed in the binder mock-ups (Figure 3a). Thus, in the R-mock-up, reflectance increased across the whole spectrum, but, in the E-mock-up, a decrease was recorded above all in the region from 450 to 600 nm.

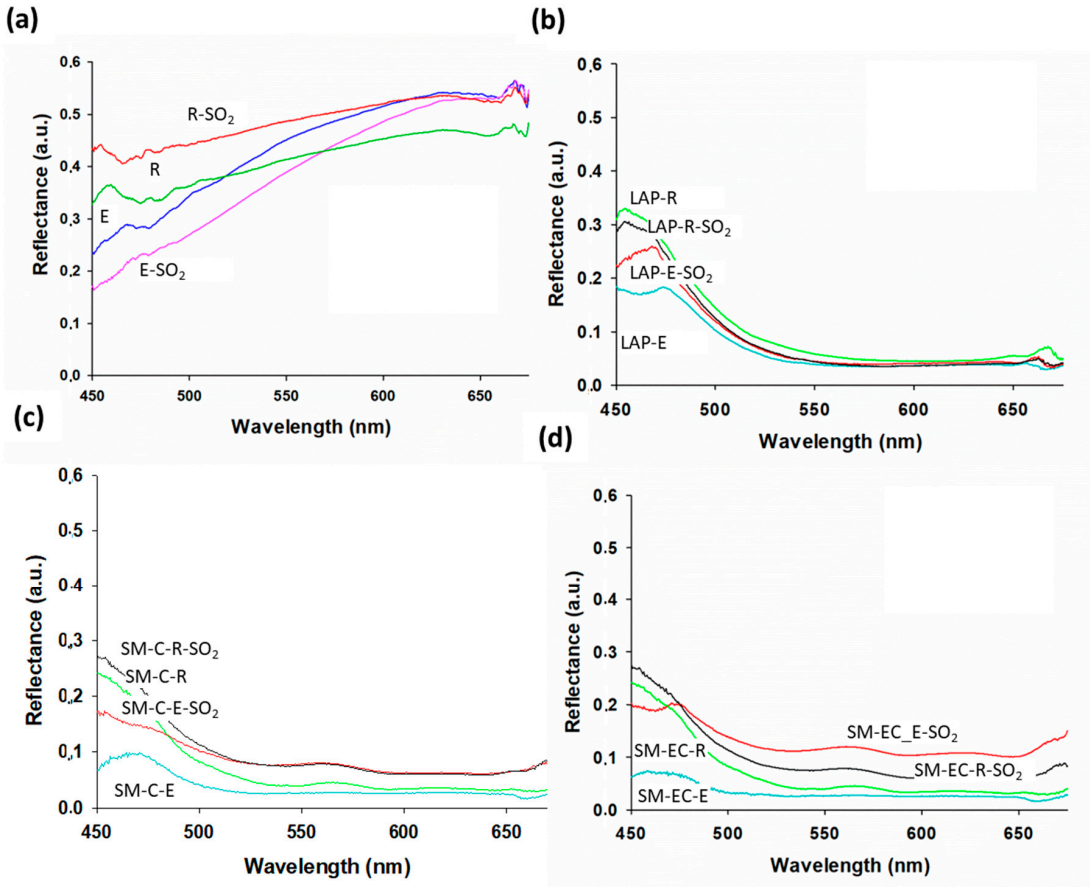

Figure 3. Reflectance spectra of the binder mock-ups (**a**), LAP-based mock-ups (**b**) and SM-based mock-ups with different grain sizes, i.e., coarse (**c**) and extra-coarse (**d**). Check Table 1 to better follow the paints labeling. $-SO_2$ shows the aged samples.

Regarding tempera mock-ups, different behaviors were observed, depending on the pigment, the binder, and the grain size of the pigment. In the LAP-mock-ups (Figure 3b), the changes in reflectance affected the blue region of the spectrum and varied depending on the binder present in the paint: in LAP-E paint, the reflectance value increased, while it fell in LAP-R paint. All of the SO_2 aged SM-mock-ups showed higher reflectance than their fresh counterparts, irrespective of the binder present in the paint (Figure 3c,d). Additionally, in SM-paints reflectance varied, depending on the pigment grain size. In paints made with coarse pigment (SM-C), exposure to SO_2 caused an increase in reflectance in SM-paints, regardless of the binder. This increase occurred in the blue region and in the rest of the spectrum from 500 nm up to 650 nm, as shown in Figure 3c. An increase in reflectance also occurred in paints that were prepared with extra-coarse smalt grains (SM-EC), affecting above all the region between 500 nm and 650 nm (outside the blue region), particularly in the SM-EC-E paint (Figure 3d). The influence of the grain size on the reflectance was previously reported for tempera paint mock-ups in Pozo-Antonio et al. [22]. It should be noted that SM-EC-based paints underwent the most intense color change towards whitening, as observed with the stereomicroscope (Figure 1). This whitening results in a change in the tone away from the blue and, therefore, it is logical that a change in the reflectance would manifest itself in a region other

than the blue region. This variation in reflectance coincides with the modification in the b* coordinate noted in these paints. Surface salt formation is undoubtedly behind these changes in reflectance, but the following facts could indicate differential deterioration related to interaction between pigment and binder or even to chemical deterioration of the pigments: (1) the reflectance changes are different (in intensity and direction) between the LAP-based and SM-based paints and (2) differences between grain sizes of SM pigment were also found.

Figure 4 shows the FTIR spectra of selected representative paint and binder mock-ups that were studied in this work. The typical functional groups that characterize both binders, i.e., egg yolk (E) and rabbit glue (R), were identified in the FTIR spectra of the fresh binder mock-ups and the fresh tempera mock-ups. In fresh E-based temperas, the following bands were detected: 3264 cm^{-1} assigned to the N–H stretching, 2920 cm^{-1} ($\nu_{AS}(CH_2)$ stretching from long chain fatty acids), 2850 cm^{-1} ($\nu_{S}(CH_2)$ stretching from long chain fatty acids), 1735 cm^{-1} assigned to C = O asymmetric stretching, 1620 cm^{-1} (ν(C = O) stretching from amide I), and 1517 cm^{-1} (ν(N–H) bending from amide II) [58–60]. The FTIR bands that were assigned to rabbit glue (Figure 4) were those found at 3280 and 3075 cm^{-1}, corresponding to N-H stretching, at 2929 cm^{-1} ($\nu_{AS}(CH_2)$ stretching from long chain fatty acids), a weak shoulder at 2870 cm^{-1} ($\nu_{S}(CH_2)$ stretching from long chain fatty acids), at 1630 cm^{-1} assigned to C = O stretching from amide I, at 1542 cm^{-1} assigned to CN stretching and NH bending from amide II, and bands at 1450–1000 cm^{-1} (collagen absorption features that were attributed to CH_2 wagging, CH_3 deformation, C–N stretching, and C–OH stretching) [23,60–62]. After the SO_2 aging test, no large variations were detected in the typical FTIR bands of the binders, although a slight band (absent in the fresh samples) was identified at 1090 cm^{-1}, which could be due to S–O stretching. This finding confirms that sulfate was formed on the binder surfaces as a consequence of SO_2 exposure.

The FTIR spectrum of fresh LAP-E paint (Figure 4) showed a shoulder in the range 1100–1050 cm^{-1}, a band at 960 cm^{-1} assigned to O–Si–O antisymmetric stretching vibrations, bands in the range 669–597 cm^{-1} that could be assigned both to the S-O group and to Si–O, and an intense band at 410 cm^{-1} that was assigned to the O-Si-O deformation mode [62–65]. Hence, FTIR confirmed the XRD findings that the LAP pigment used in this study was not composed of haüynite, as indicated by *Kremer*, as it did not contain the band at 1149 cm^{-1} due to SO_4^{2-}, which is characteristic of haüynite-type lapis lazuli [64]. Moreover, the lack of the sharp stretching band at 2340 cm^{-1} assigned to CO_2 revealed that this LAP pigment was not from Afghanistan [65], although this is the source specified by the manufacturer. As regards the fresh SM-based mock-ups, their FTIR spectra detected potassium silicate glass by means of bands at 987 cm^{-1} assigned to the O–Si–O antisymmetric stretching mode and 410 cm^{-1} assigned to the O–Si–O deformation mode [62].

After the SO_2 test (Figure 4), the following bands that were assigned to the S–O group were detected in the FTIR spectra for the aged mock-ups: i) in LAP-E-SO_2, LAP-R-SO_2, SM-C-E-SO_2, and SM-EC-E-SO_2, a strong band at 1090 cm^{-1} assigned to S–O stretching, and ii) in all SM-based paints, an intense band at 613 cm^{-1} assigned to S–O bending vibration. In addition, in the aged LAP-based paints bands were identified at 3500 cm^{-1} and 3372 cm^{-1} and assigned to OH stretching of water. This pair of bands is characteristic of hydrated sulfated salts, especially gypsum [66]. Therefore, these findings confirm the XRD results indicating the presence of hydrated sulfated salts, such as those identified in aged LAP-paints, namely gypsum, bassanite, and pentahydrite.

It is worth noting that no noticeable variations in the typical FTIR bands of the binders were detected in the SO_2 aged paints, except in the SM-based paints made with rabbit glue (see Figure 4). In these samples, a decrease in the characteristic rabbit-glue FTIR bands was detected, especially in the 1630 cm^{-1} band (C = O stretching) and the shoulder ca. 3280 cm^{-1} (corresponding to N–H stretching). These results agree with the SEM findings explained below, in that rabbit-glue binder seems to dissolve in the aged paints, most likely due to the humidity conditions of the SO_2 test.

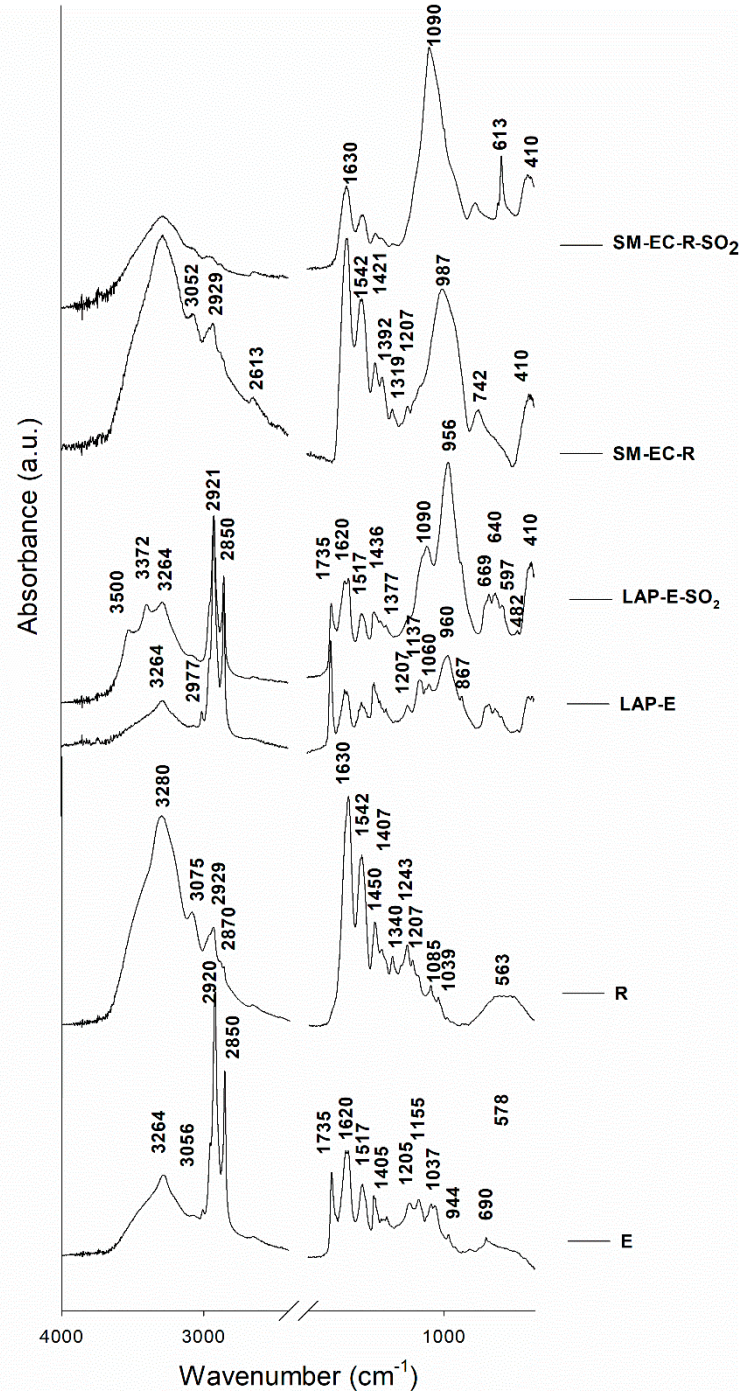

Figure 4. Attenuated Transmittance Reflectance–Fourier transform infrared spectroscopy (ATR-FTIR) (absorbance) spectra of the most representative paint and binder mock-ups in this research. Check Table 1 to better follow the paints labeling. $-SO_2$ shows the aged samples.

Figure 5 shows the surface of representative tempera mock-ups before and after exposure to SO_2 as well as the aged R-mock-up (made solely with rabbit glue) studied with SEM-EDS. Note the clear difference in the surface texture of the fresh paints, which mainly varies according to the binder used in the tempera, irrespective of the pigment it contains. Thus, the R-based paints (made with either pigment) showed rougher and seemingly more porous surfaces than the paints that were made with E, so much so that it was possible to distinguish the pigment grains protruding from the glue binder. This finding suggests that the agglutination and coating capacity of the R binder is lower than that

of the E binder. Similar situations in which the pigment particles were not completely covered by animal glue have also been observed in previous research studies [23,24,35]. The E binder, by contrast, has been shown to cover the pigments well [24].

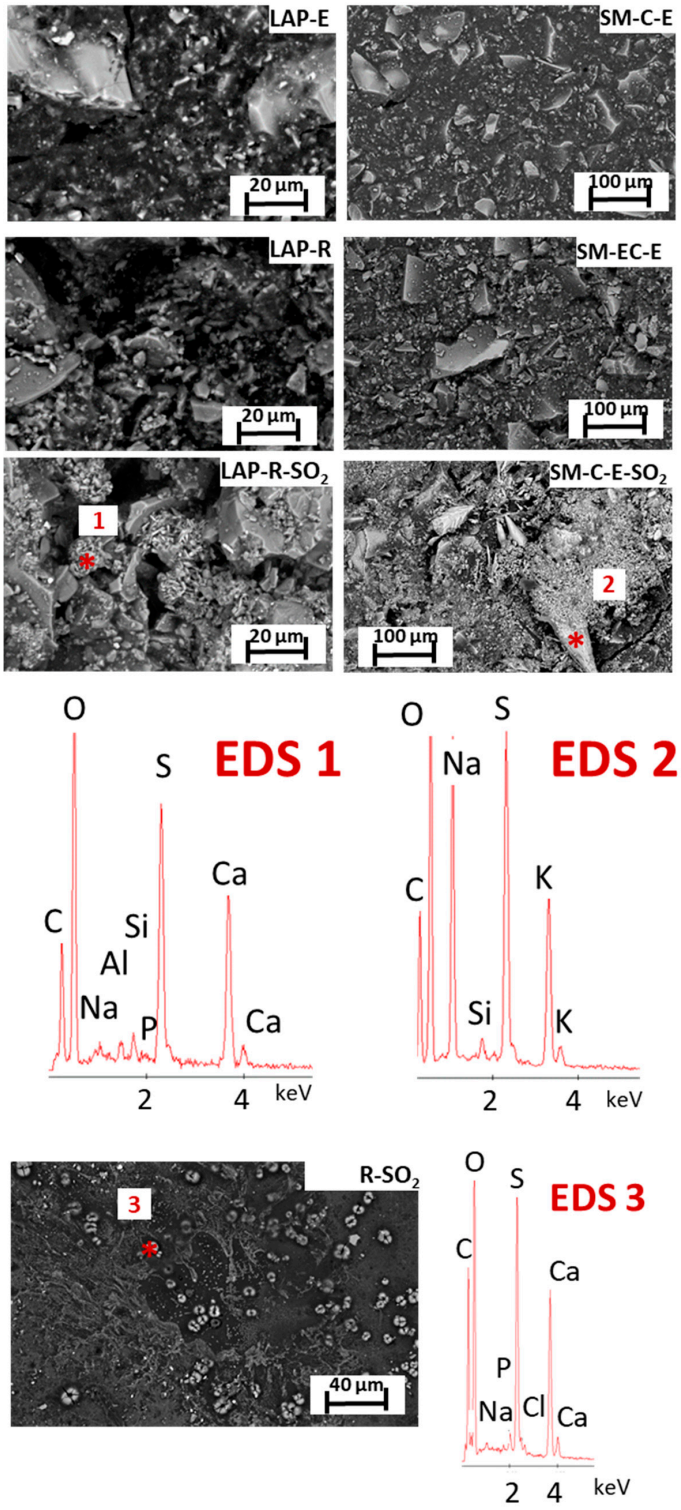

Figure 5. Scanning electron microscope (SEM) micrographs and energy-dispersive X-ray spectroscopy (EDS) spectra of LAP- and SM-paint mock-ups, before and after the SO_2 aging test. Also shown is the SO_2 aged rabbit glue (R) mock-up. Check Table 1 to better follow the paints labeling. $-SO_2$ shows the aged samples.

SEM observation also allowed for us to identify the morphological features of the pigments (Figure 5). Thus, for the LAP pigment, we observed crystals of different sizes with the angular/irregular edges typically observed in powder that was obtained by grinding larger lumps of rock. This denotes the natural origin of the lapis lazuli, which is further corroborated by the associated impurities that were identified with XRD and FTIR.

From a chemical point of view, the lazurite crystals on the LAP-based mock-ups were identified by EDS through the detection of sodium (Na), aluminum (Al), silicon (Si), sulfur (S), and calcium (Ca), whereas the SM pigment in the SM-based paints was identified through EDS spectra rich in Si, K, and Co. Na was also found in this glass-rich pigment. This ion is related to the addition of Na carbonate, besides K carbonate, as raw material in glass production. For its part, phosphorus (P) was identified in all of the E-based paint mock-ups, and probably comes from the phospholipids present in the E binder [33].

After the SO_2 test, the SEM study confirmed the precipitation of sulfate-based salts on the surface of all the tempera mock-ups and revealed that the precipitation of sulfate-rich salts also occurred in binder (E and R) mock-ups (R-mock-up in the Figure 5, EDS3 spectrum). Crystal deposits rich in S and Ca and, to a lesser extent, in Na, Cl and P were identified showing different habits, i.e., acicular, tabular, and cell-shaped. These findings are consistent with the FTIR results that revealed the existence of sulfate compounds on the binder mock-ups through the detection of bands that were assigned to the S-O group. Na and Cl were identified in the binder mock-ups (attributed to NaCl), which might have come from the water used in the SO_2 test (when considering the amount of both Cl^- and Na^+, which are 15.8 mg/L and 13.18 mg/L, respectively).

In tempera mock-ups, globular-shaped deposits that formed by acicular crystals rich in Ca and S were detected on the surfaces of aged LAP-mock-ups (Figure 5, EDS1); these deposits probably correspond to gypsum and bassanite identified by means of XRD. As regards aged SM-based paints, four types of neoformed compounds were identified on their surfaces (Figure 5 and the EDS2): (i) horn shaped crystals that are rich in Na, S, and K, which could be assigned to aphthitalite already identified by XRD; (ii) a few μm- length aciculae, rich in Na, S, and K, which could also be assigned to aphthitalite; (iii) regular structures rich in S, K, and Ca or S, K, and Na, and (iv) abundant deposits that are rich in S and K. The varied chemical balances indicate the possible coexistence of different sulfate species, although only thenardite and aphthitalite were identified with XRD (see Table 1). It is important to note that surface SEM observations did not reveal a higher amount of salt deposits on SM-based mock ups when compared to LAP-based mock ups, which would explain the whitening suffered by SM temperas. Similarly, a greater amount of saline deposits has not been found in the SM-E-mock-ups that could explain the greater whitening of these paints when compared to the SM-R-mock-ups. Thus, the hypothesis previously stated, i.e., the more intense whitening of SM-E paints compared to SM-R paints due to a higher salt precipitation on SM-E paint surfaces, must be ruled out.

Figure 6 shows the micrographs of selected fresh and aged LAP- and SM-mock-ups prepared as thin sections and studied under PLM and SEM-EDS. In accordance with the previous SEM results, we observed that the surface of the fresh E-based paints (with a thickness of ca. 110–120 μm) was more continuous than that of the fresh R-based paints. The surface was also smoother, as the pigments grains were well covered by the E binder (Figure 6), in contrast to the paints made with R, in which the pigments grains stood out from the binder matrix, as if floating on the surface of the paint (see SM-EC-R-Ref and SM-EC-R-SO_2 micrographs in Figure 6). Therefore, the R-based paints (both with LAP and SM pigments) displayed rougher, more porous surfaces with a wider range of thicknesses (70–120 μm).

After SO_2 exposure, yellowing and opacification of the E binder was observed under PLM in aged E-based paints (LAP-E-SO_2, SM-EC-E-SO_2, Figure 6). In R-based paints, yellowing has not been observed, but, by contrast, new pores were formed apparently due to loss of binder. Thus, the cohesion of the paint layer in E-based paints remained almost intact, after the SO_2 test (as only slight fissures were detected on the binder, Figure 6-LAP-E-SO_2, SM-EC-E-SO_2); conversely, R-based paints lost much

of the binder, leaving the surface rough and the pigment grains exposed (Figure 6, SM-EC-R-SO_2). The physical deterioration that was suffered by rabbit glue binder in the tempera mock-ups could contribute to the changes in the reflectivity that the paints underwent after the SO_2 test. In fact, De la Rié et al. [67] pointed out that the changes in reflectance shown on lapis lazuli model paints after UV ageing were due the micro-cracking suffered in the binder, which improves light scattering. Additionally, the cracking of rabbit glue used as binder on tempera mock-ups was already described previously by other authors; in [23], polygonal cracks were observed in UV-aged rabbit glue-based paints mock-ups that were prepared with azurite of different grain sizes, with this cracking being more intense in paints made with coarser pigments (grain sizes from 63 to 100 μm) than in those made with pigments with smaller grain sizes (<63 μm).

The deterioration of rabbit glue that was observed under SEM agrees with FTIR results, which showed a significant reduction in the intensity of the characteristic rabbit glue FTIR bands in the paint mock-ups containing this binder. It is noteworthy the fact that the intensity and type of degradation of the glue binder in SM-based paints were the same, regardless of the grain size of the pigment. These results indicate that the rabbit glue binder is more susceptible than egg yolk binder to decay processes in terms of binder loss, associated with exposure to an SO_2 atmosphere.

Furthermore, the SEM study allowed us to confirm three facts:

(i) in all paint mock-ups, noteworthy amounts of S and Ca were found not only on the surface of the paints, but also within paint layers, as well as smaller amounts of Mg in LAP-paints and Na and K in SM-paints. The pressure that is generated by the precipitated sulfated salts could have contributed to the binder damage by enhancing its cracking. In this regard, the lipid-rich composition of the egg yolk could provide greater resistance to salt crystallization, since the fatty binder will confer a hydrophobic character on the paints. We measured the static contact angle (SCA) of fresh LAP- and SM-based paints to verify this hypothesis. Surprisingly, the only paint with an SCA greater than 90° was LAP-R (115°). Note that the SCA was 85° for LAP-E paint. All of the SM-based paints had SCA values of less than 90° (ranging between 20° and 40°) and, contrary to our expectations, the SCA values of the R-based paints were slightly higher than those of the E-based paints. This might be related with the findings that were observed with SEM and PLM, in that the R-based paints were not so good at covering the pigment grains, therefore leaving more exposed, unprotected pigment grains with irregular edges when compared to E-based paints. Subsequently, R-based paints showed higher Rz than their E–based counterparts (with the exception of SM-EC paints in which there were no statistically significant differences in Rz values). Therefore, the higher SCA values in these R-based paints are predictable, since the higher the roughness, the higher the SCA, which, in turn, means that these paints are more hydrophobic [68,69].

(ii) No evidence of chemical deterioration (pitting, dissolution symptoms, etc.) has been found in the lapis lazuli grains mixed with either E or R binder of LAP-paints. This fact raises a question regarding the source of the cations that make up the different sulfate salts that are found in the LAP- paints, especially the Mg, which is present in negligible amounts in the water used in the test. The hypothesis that the Mg ion comes from the alteration of the diopside present in trace amounts in the LAP pigment is therefore reinforced. As previously indicated, the stability of diopside in the alteration environment of this SO_2 test is lower than lapis lazuli. Moreover, Ca from bassanite could also come from calcite, which is chemically unstable at the characteristic acidic pH of the sulfation process from SO_2 gas. Indeed, previous research found that the calcite present in paints mock-ups made with either egg yolk or rabbit glue reacted with SO_2, under natural and accelerated SO_2 aging tests, in order to form calcium sulfite/sulfate [11]. However, we could not detect deterioration symptoms in diopside and calcite grains on aged LAP-based paints while using SEM. These two minerals are present in the LAP temperas as very small grains. Therefore, their mixture with the binder makes difficult their observation and chemical analysis. The visualization of these grains separately of the organic phase, or applying TEM analysis would be two appropriate strategies for confirming that Mg and Ca were released from these two accessory minerals.

Although we cannot confirm the dissolution of calcite in LAP-paints, the formation of pentahydrite can be considered to occur at the expense of the diopside due to the fact that the Mg^{2+} content of the water used was very low. The contribution of the impurities in the lapis lazuli pigment to the aging susceptibility of tempera model paints has not yet been fully examined in the specialist literature, even though impurities affect the final color of the natural pigment, the chemical-physical properties, and, therefore, its resistance to alteration, as found in the present study and elsewhere [22,26,27]. Hence, the use of impurity-free synthetic ultramarine instead of (natural) lapis lazuli could be a satisfactory preventive conservation strategy in restoration campaigns. In the literature, previous efforts aimed to obtain acidic-resisting ultramarine pigments by means of a novel two-step silica coating process [70] or by incorporating white lead or amine compounds as light stabilizers [67]. However, these contributions focus on the protection of ultramarine pigments against acid attack and UV light, but not against SO_2 attack.

(iii) A chemical alteration was confirmed in the SM pigments. The degree of chemical deterioration was evaluated while using K/Co ratios following a previous work [41], in which K leaching from the smalt glass structure has been related to K/Co < 1, so that fresh blue smalt grains presented K/Co higher than 1, whereas aged pale smalt grains had K/Co ratio as low as 1/4. In the present work, K and Co concentrations were obtained with the energy dispersion microprobe coupled to SEM (i.e., SEM-EDS). A minimum of 20 analyses were performed on SM grains from paints made with both binders (E and R) before and after the SO_2 test. In fresh E-based paints, 100% of the analyses performed on SM grains had K/Co ≥ 1; in fresh R-based paints, only 85% of the analyses had K/Co > 1. After the SO_2 test, the K/Co ratio was higher or similar to 1 in only 30% of analyses made. It is important to note that this proportion occurred in similar percentages in both E- and R-based paints, regardless the grain size of the smalt pigment.

These results confirm, firstly, that there has been a leaching of K from smalt grains after exposure to SO_2, strengthening the hypothesis that the K forming the aphthitalite salt ($K_3Na(SO_4)_2$) in the SM-R-based paint comes from the smalt itself. On the other hand and, according to other authors [41,42], the leaching of K could be the reason for the whitening of the SM-based paints after SO_2 exposure. As previously stated, this whitening was unlikely to be solely due to the deposition of salts, since these salts were found in similar amounts in LAP- and SM-based paints, but only the latter lost its characteristic blue color. However, it is difficult to explain the reason why the SM-E paints have suffered more whitening than SM-R paints (see Figure 1). Two hypotheses were previously proposed here in order to explain the more intense whitening in SM-E paints: (1) a greater quantity of saline deposits. However, in SM-E paints, this possibility must be ruled out, since SEM did not show a greater amount of salt deposits in these paints, (2) a release of K from the glass structure favored by the acidic to neutral environment generated by the fatty acids of the egg yolk, which is the hypothesis that is offered in other works [40]. This hypothesis could not be considered in the current study, since the percentage of cases in which the K/Co ratio was lower than 1 was similar in the paints made with both binders. A feasible explanation for the color difference between the SM-based paints with egg yolk and those with rabbit glue, given that they differed neither in salt content nor in the degree of K release, is mainly the different deterioration suffered by each binder. Indeed, the yellowing and opacification of the egg yolk must undoubtedly contribute to the color change in these paints. Note that the rabbit glue binder did not change color in the aged mock-ups. Noteworthy is the fact that the intense degradation of the rabbit glue in aged R-based tempera (leaving the pigment grains exposed, see Figure 6 and related comments) did not favor a greater chemical deterioration of smalt grains, since smalt K/Co ratios after the SO_2 test were similar in SM-based paints with both binders.

The results of the SEM analysis, which confirm the different susceptibility of both pigments to the SO_2 aging test, clarify the importance of the chemical structure (and, consequently, the main mechanism of deterioration) of the pigments in the durability of the tempera paints. Thus, the differences between pigments regarding their mechanisms of alteration could even explain the interesting fact that the salts formed in LAP-paints are hydrated (pentahydrite, gypsum, and bassanite) whereas the salts that formed in SM-paints are anhydrous. On the one hand, lazurite that is present in the pigment lapis lazuli

is a tectosilicate (likewise ultramarine) made by a resistant aluminosilicate framework, built with AlO_4 and SiO_4 tetrahedral units linked by shared oxygen atoms and sodium cations. These cubic-octahedral cavities, also called β-cages, are able to trap and stabilize the sulfur radical anions, i.e., S_3^- and S_2^-, which are responsible for the pigment blue color. The strength of the bonds makes this structure quite stable against hydrolysis, which, consequently, would progress very slowly, causing a low ion exchange between the water and the mineral ions. The water present in the SO_2 test environment would have interacted with the impurities of calcite and diopside contained in the LAP pigment, most probably leading to the precipitation of hydrated salts rich in the ions leached out from the mentioned minerals. On the other hand, the smalt pigment, being a glass, is an amorphous solid whose corrosion is a complex and slow process (which has been accelerated in the SO_2 test conducted here) that involves a diffusion and exchange of ions from the surface to the interior. The process begins with the adsorption of water on the glass surface; protons diffuse within the glass structure and they are exchanged with alkali metal ions present, especially Na. Hydroxyl accumulation generates a pH increase that favors the breakage of the Si–O–Si bond that hydrolyzes, forming silica gel. In this process, water plays an active role, so that it is not available for the formation of hydrated salts, thus becoming part of silica gel. Consequently, the probability of hydrated salts precipitating is low. However, the process is not so simple. In addition to the actual deterioration of the smalt pigment, other variables to consider are: the contribution of each binder to the deterioration of the tempera paints (which is different, depending of the binder nature), as has been corroborated in this study, the binder-pigment interaction under the SO_2 aging test, and, finally, the role of impurities and their different stability to weathering.

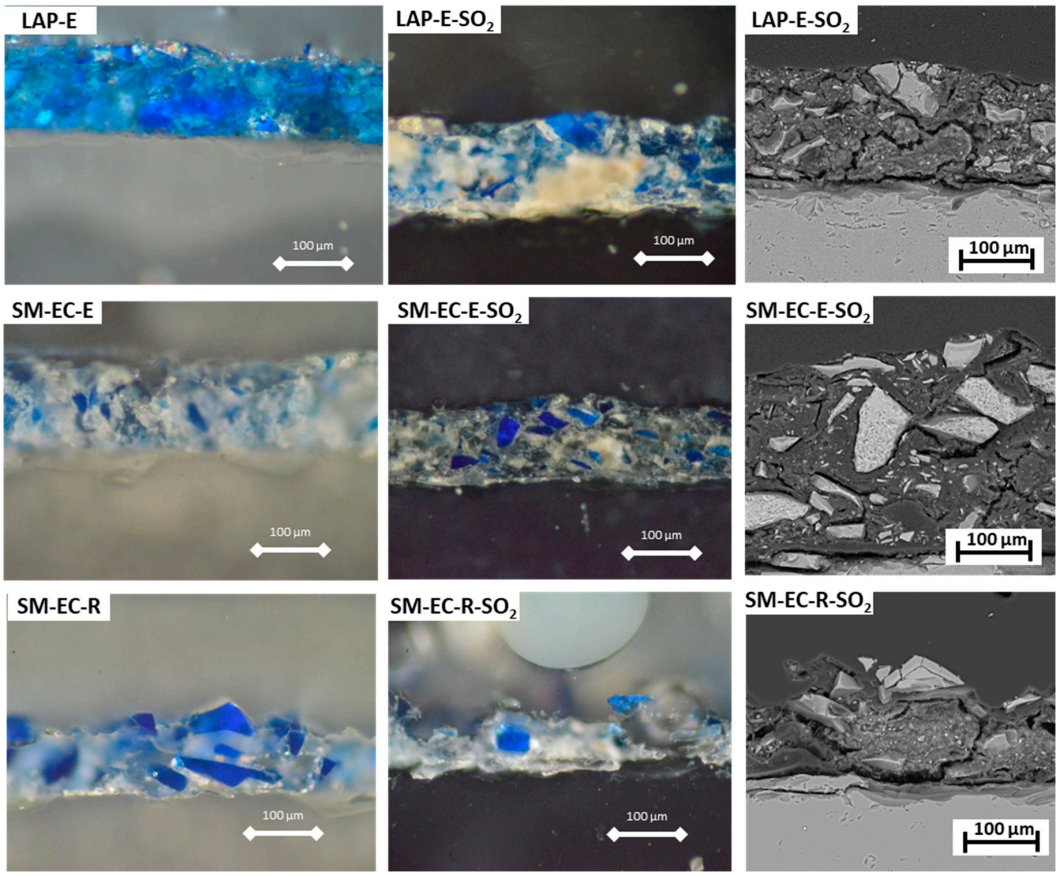

Figure 6. Micrographs taken with polarized light microscope (PLM) (left and center) and SEM (right) of cross-sections of selected tempera paint mock-ups made with lapis lazuli (LAP) or smalt (SM) mixed with either egg yolk (E) or rabbit glue (R) before and after SO_2 exposure. Center and right columns showed micrographs of the same part of the tempera mock-ups. Check Table 1 to better follow the paints labeling. –SO_2 shows the aged samples.

4. Conclusions

The results that were obtained in this study led us to draw the following conclusions:

Fresh lapis lazuli- or smalt-based tempera mock-ups presented, before the exposure to SO_2, different textures, which were primarily induced by the different binders used in the tempera. The egg yolk-based paints had more compact and continuous layers than those that were made with rabbit glue. Rabbit glue binder had a more limited grain agglutination capacity than the egg yolk binder. Moreover, fresh egg yolk-based paints had a more faded yellow color than those that were made with rabbit glue, which showed greater reflectance.

After the SO_2 aging test, calcium and magnesium sulfates were formed in lapis lazuli-based paints and sodium and potassium-sodium sulfates were formed in smalt-based paints; deposits rich in S, Ca, Na, P, and Cl were also formed on the mock-ups solely made with binders. The sulfation process was active not only on the surface of the paint mock-ups but also inside the paint layers, as indicated by the neoformed sulfate salts. No clear relation was found between the type of binder (egg yolk or rabbit glue) and the variations in gloss and roughness, despite the fact that the fresh rabbit glue paints were rougher than those made with egg yolk. The SO_2 test produced imperceptible color changes to the naked eye on lapis lazuli temperas, while intense whitening was observed on smalt-based paints. Colorimeter measurements also confirmed that variations in color in the egg yolk-based paints were greater than in the rabbit glue-based paints, especially in the temperas containing smalt. Paints reflectance was also modified after the SO_2 test; in smalt based-paints, reflectance increased in all of the cases, but to a greater extent when egg yolk was used as binder. Salt precipitation on the paint surface contributed to color and reflectance variations in the paints that were subjected to SO_2 exposure.

Deterioration was confirmed both in binders and in pigments. Regarding binders, egg yolk suffered yellowing and opacification, being—in the case of tempera made with lapis lazuli—the responsible for the weak color change suffered by this paint. In rabbit glue-based paints, the loss of binder creating new pores was observed.

For lapis lazuli-based paints, lazurite grains remained unaltered. Hence, the deterioration of these paints was related to: (1) the deterioration of the binders: yellowing in egg yolk-based tempera and lost in rabbit glue-based tempera and (2) the deterioration of the trace minerals present in the pigment, i.e., calcite and diopside. Thus, the origin of Mg^{2+} of the pentahydrite detected after the test was related to the hydrolysis of diopside, given that no other source of Mg is likely, whereas the Ca^{2+} of bassanite and gypsum could be related to the dissolution of calcite. Further analysis must be conducted to identify the features (chemical or morphological) that support these assertions. On the basis of these findings, a recommendation can be established to avoid salt precipitation on the surface of lapis lazuli rich paintings exposed to polluted SO_2-rich atmospheres, that is, the use of impurity-free synthetic ultramarine pigment instead of lapis lazuli. Similarly, we recommend cleaning off from the paint surface the efflorescence produced by exposure to SO_2 to restore the color saturation in the lapis lazuli-based paints.

Smalt pigment in tempera paints made either with egg yolk or rabbit glue revealed greater susceptibility to SO_2 attack than the lapis lazuli pigment. Indeed, smalt suffered a chemical deterioration, evidenced through the K^+ leaching from the glass matrix. This process, as confirmed by the K/Co ratio reduction, induced both the loss of blue coloration in smalt-based tempera and salt precipitation on the surfaces of the paints. The opacification and yellowing of the egg yolk binder after the SO_2 test could explain the more intense blue color loss in the smalt tempera made with egg yolk. The results confirmed that the resistance of the smalt-based tempera to SO_2 exposure is independent of the grain sizes of the pigment. However, taking into account that: (1) in the present work, smalt-based tempera showed greater susceptibility to SO_2 attack when compared to the lapis lazuli-based tempera and (2) previous works have demonstrated the greater stability of ultramarine pigments when compared to other blue pigments, it could be suggested that, during restoration work of paintings, the replacement

of smalt by ultramarine pigments—or mixtures of both to get the right color—could be considered as a preventive strategy in order to slow down the deterioration.

Author Contributions: Conceptualization, J.S.P.-A., C.C. and T.R.; methodology, J.S.P.-A., D.B., A.D., T.R. and C.C.; software, J.S.P.-A., T.R. and D.B.; validation, J.S.P.-A., T.R. and C.C.; formal analysis, J.S.P.-A., D.B., T.R., C.C.; investigation, J.S.P.-A., D.B., A.D., T.R. and C.C.; resources, C.C., A.D. and T.R.; data curation, J.S.P.-A., D.B., T.R. and C.C.; writing—original draft preparation, J.S.P.-A., T.R., D.B. and C.C.; writing—review and editing, J.S.P.-A., C.C. and A.D.; visualization, J.S.P.-A., C.C and T.R.; supervision, J.S.P.-A. and C.C.; project administration, J.S.P.-A., C.C.; funding acquisition, T.R., C.C. and A.D. All authors have read and agreed to the published version of the manuscript.

Funding: This research was funded by Spanish Research Projects AERIMPACT (CGL2012–30729) and EXPOAIR (P12-FQM-1889), the European Regional Development Fund (ERDF) and the Andalusian Research Group RNM-179. J. Santiago Pozo-Antonio thanks the Spanish Ministry of Economy and Competitiveness (MINECO) for his "Juan de la Cierva-incorporación" (IJCI-2017-3277) post-doctoral contract.

Acknowledgments: The authors would like to acknowledge the contributions made by Ana Mato and Lara de Villalobos in the acquisition and curation of the data. They also acknowledge the support of the CERENA (strategic project FCT-UID/ECI/04028/2019). Analyses were performed in the CACTI (Centro de Apoyo a la Investigación) Research Support Centre at the University of Vigo. Accelerating SO_2 aging test were performed in Instituto Superior Tecnico (University of Lisbon, Portugal).

Conflicts of Interest: The authors declare no conflict of interest.

References

1. European Environment Agency. *Air Pollution Fact Sheet 2013—Spain*; European Environment Agency: Copenhagen, Belgium, 2013.
2. Cotte, M.; Susini, J.; Metrich, N.; Moscato, A.; Gratziu, C.; Bertagnini, A.; Pagano, M. Blackening of Pompeian Cinnabar Paintings: X-ray Microspectroscopy Analysis. *Anal. Chem.* **2006**, *78*, 7484–7492. [CrossRef]
3. Maguregui, M.; Knuutinen, U.; Martínez-Arkarazo, I.; Castro, K.; Madariaga, J.M. Thermodynamic and spectroscopic speciation to explain the blackening process of hematite formed by atmospheric SO_2 impact: The case of Marcus Lucretius House (Pompeii). *Anal. Chem.* **2011**, *83*, 3319–3326. [CrossRef]
4. Urosevic, M.; Yebra-Rodríguez, A.; Sebastián-Pardo, E.; Cardell, C. Black soiling of an architectural limestone during two-year term exposure to urban air in the city of Granada (S Spain). *Sci. Total Environ.* **2012**, *414*, 564–575. [CrossRef]
5. Sabbioni, C. Contribution of atmospheric deposition to the formation of damage layers. *Sci. Total Environ.* **1995**, *167*, 49–55. [CrossRef]
6. Brimblecombe, P.; Grossi, C.M. Aesthetic thresholds and blackening of stone buildings. *Sci. Total Environ.* **2005**, *349*, 175–189. [CrossRef] [PubMed]
7. Rivas, T.; Pozo, S.; Paz, M. Sulphur and oxygen isotope analysis to identify sources of sulphur in gypsum-rich black crusts developed on granites. *Sci. Total Environ.* **2014**, *482*, 137–147. [CrossRef] [PubMed]
8. Charola, A.E.; Ware, R. Acid deposition and the deterioration of stone: A brief review of a broad topic. *Geol. Soc. Spec. Pub.* **2002**, *205*, 393–406. [CrossRef]
9. Maravelaki-Kalaitzaki, P. Black crusts and patinas on Pentelic marble from the Parthenon and Erechtheum (Acropolis, Athens): Characterization and origin. *Anal. Chim. Acta* **2005**, *532*, 187–198. [CrossRef]
10. La Russa, M.F.; Fermo, P.; Comité, V.; Belfiore, C.M.; Barca, D.; Cerioni, A.; De Santis, M.; Barbagallo, L.F.; Ricca, M.; Ruffolo, S.A. The Oceanus statue of the Fontana di Trevi (Rome): The analysis of black crust as a tool to investigate the urban air pollution and its impact on the stone degradation. *Sci. Total Environ.* **2017**, *593–594*, 297–309. [CrossRef] [PubMed]
11. Herrera, A.; Cardell, C.; Pozo-Antonio, J.S.; Burgos-Cara, A.; Elert, K. Effect of proteinaceous binder on pollution-induced sulfation of lime-based tempera paints. *Prog. Org. Coat.* **2018**, *123*, 99–110. [CrossRef]
12. Mayer, R. *Materiales y Técnicas del Arte*; Hermann Blume: Madrid, Spain, 1985; p. 687.
13. Cardell-Fernández, C.; Navarrete-Aguiler, C. Pigment and Plasterwork Analyses of Nasrid Polychromed Lacework Stucco in the Alhambra (Granada, Spain). *Stud. Conserv.* **2006**, *51*, 161–176. [CrossRef]
14. Cardell, C.; Rodriguez-Simon, L.; Guerra, I.; Sanchez-Navas, A. Analysis of Nasrid polychrome carpentry at the Hall of the Mexuar Palace, Alhambra complex (Granada, Spain), combining microscopic, chromatographic and spectroscopic methods. *Archaeometry* **2009**, *51*, 637–657. [CrossRef]

15. Gonzalez-Cabrera, M.; Arjonilla, P.; Domínguez-Vidal, A.; Ayora-Cañada, M.J. Natural or synthetic? Simultaneous Raman/luminescence hyperspectral microimaging for the fast distinction of ultramarine pigments. *Dye. Pigment.* **2020**, *178*, 108349. [CrossRef]
16. Dominguez-Vidal, A.; De la Torre-López, M.J.; Campos-Suñol, M.J.; Rubio-Domene, R.; Ayora-Cañada, M.J. Decorated plasterwork in the Alhambra investigated by Raman spectroscopy: Comparative field and laboratory study. *J. Raman Spectrosc.* **2014**, *45*, 1006–1012. [CrossRef]
17. Dominguez-Vidal, A.; De la Torre-Lopez, M.J.; Rubio-Domene, R.; Ayora-Cañada, M.J. In situ noninvasive Raman microspectroscopic investigation of polychrome plasterworks in the Alhambra. *Analyst* **2012**, *137*, 5763. [CrossRef]
18. Su, Y.; Ji, M.; Li, J.; Chang, C.; Dong, S.; Deng, Y.; Yang, Y.; Gu, L. Subcritical fluid extraction treatment on egg yolk: Product characterization. *J. Food Eng.* **2020**, *274*, 109805. [CrossRef]
19. Schellmann, N.C. Animal glues: A review of their key properties relevant to conservation. *Rev. Conserv. Stud.* **2007**, *8*, 55–66. [CrossRef]
20. Palet, A. *Tratado de Pintura: Color, Pigmentos y Ensayo*; Edicions Universitat de Barcelona (UB): Barcelona, Spain, 2002; p. 172.
21. Rivas, T.; Pozo-Antonio, J.S.; Barral, D.; Martínez, J.; Cardell, C. Statistical analysis of colour changes in tempera paints mock-ups exposed to urban and marine environment. *Measurement* **2018**, *118*, 298–310. [CrossRef]
22. Pozo-Antonio, J.S.; Barral, D.; Herrera, A.; Elert, K.; Rivas, T.; Cardell, C. Effect of tempera paint composition on their superficial physical properties- application of interferometric profilometry and hyperspectral imaging techniques. *Prog. Org. Coat.* **2018**, *117C*, 56–68. [CrossRef]
23. Cardell, C.; Herrera, A.; Guerra, I.; Navas, N.; Rodríguez Simón, L.; Elert, K. Pigment-size effect on the physico-chemical behavior of azurite-tempera dosimeters upon natural and accelerated photo aging. *Dye. Pigment.* **2017**, *141*, 53–65. [CrossRef]
24. Elert, K.; Cardell, C. Weathering behavior of cinnabar-based tempera paints upon natural and accelerated aging. *Spectrochim. Acta Part A Mol. Biomol. Spectrosc.* **2019**, *226*, 236–248. [CrossRef] [PubMed]
25. Price, M. A renaissance of color: Particle separation and preparation of azurite for use in oil painting. *Leonardo* **2000**, *33*, 281–288. [CrossRef]
26. Pérez, M.; Castro, K.; Rodríguez, M.D.; Olazabal, M.A.; Madariaga, J.M. A critical analysis of commercial pigments. In *ART 2002, Proceedings of the 7th International Conference on Non-destructive Testing and Microanalysis for the Diagnostics and Conservation of the Cultural and Environmental Heritage, 2–6 June 2002, Antwerp, Belgium*; University of Antwerp: Antwerp-Wilrijk, Belgium, 2002; pp. 173–182.
27. Elert, K.; Herrera, A.; Cardell, C. Pigment-binder interactions in calcium-based tempera paints. *Dye. Pigment.* **2018**, *148*, 236–248. [CrossRef]
28. Katsanos, N.A.; De Santis, F.; Cordoba, A.; Roubani-Kalantzopoulou, F.; Pasella, D. Corrosive effects from the deposition of gaseous pollutants on surfaces of cultural and artistic value inside museums. *J. Hazard. Mater.* **1999**, *64*, 21–36. [CrossRef]
29. Odlyha, M.; Cohen, N.S.; Foster, G.M. Dosimetry of paintings: Determination of the degree of chemical change in museum exposed test paintings (smalt tempera) by thermal analysis. *Acta* **2000**, *365*, 35–44. [CrossRef]
30. Manzano, E.; Romero-Pastor, J.; Navas, N.; Rodríguez-Simón, L.R.; Cardell, C. A study of the interaction between rabbit glue binder and blue copper pigment under UV radiation: A spectroscopic and PCA approach. *Vib. Spectrosc.* **2010**, *53*, 260–268. [CrossRef]
31. Bacci, M.; Piccolo, M.; Porcinai, S.; Radicati, B. Tempera-painted dosimeters for environmental indoor monitoring: A spectroscopic and chemometric approach. *Environ. Sci. Technol.* **2000**, *34*, 2859–2865. [CrossRef]
32. Daniilia, S.; Minopoulou, E. A study of smalt and red lead discolouration in Antiphonitis wall paintings in Cyprus. *Appl Phys. A* **2009**, *96*, 701–711.
33. Herrera, A.; Navas, N.; Cardell, C. An evaluation of the impact of urban air pollution on paint dosimeters by tracking changes in the lipid MALDI-TOF mass spectra profile. *Talanta* **2016**, *155*, 53–61. [CrossRef]
34. Herrera, A.; Ballabio, D.; Navas, N.; Todeschini, R.; Cardell, C. Principal Component Analysis to interpret changes in chromatic parameters on paint dosimeters exposed long-term to urban air. *Chemom. Intell. Lab. Syst.* **2017**, *167*, 113–122. [CrossRef]

35. Elert, K.; Benavides-Reyes, C.; Cardell, C. Effect of animal glue on mineralogy, strength and weathering resistance of calcium sulfate-based composite materials. *Cem. Concr. Compos.* **2019**, *96*, 274–283. [CrossRef]
36. Machado, A.; Vilarigues, M. Blue enamel pigment—Chemical and morphological characterization of its corrosion process. *Corros. Sci.* **2018**, *139*, 235–242. [CrossRef]
37. Gettens, R.; Stout, G. *Painting Materials: A Short Encyclopedia*; Dover Publications: New York, NY, USA, 1966.
38. Barnett, J.R.; Miller, S.; Pearce, E. Colour and art: A brief history of pigments. *Opt. Laser Technol.* **2006**, *38*, 445. [CrossRef]
39. Delamare, F. Aux origines des bleus de cobalt: Les débuts de la fabrication du saffre et du smalt en Europe Occidentale. *Comptes Rendus Seances Acad. Inscr. Belles Lett* **2009**, *153-1*, 297–315. [CrossRef]
40. Boon, J.J.; Keune, K.; Van der Weerd, J.; Geldof, M.; Van Asperen de Boer, J.R.J. Imaging microspectroscopic, secondary ion mass spectrometric and electron microscopic studies on discoloured and partially discoloured smalt in cross- sections of 16th century paintings. *Chim. Int. J. Chem.* **2001**, *55*, 952–960.
41. Robinet, L.; Spring, M.; Pagès-Camagna, S. Vibrational spectroscopy correlated with elemental analysis for the investigation of smalt pigment and its alteration in paintings. *Anal. Methods* **2013**, *5*, 4628–4638. [CrossRef]
42. Robinet, L.; Spring, M.; Pagès-Camagna, S.; Vantelon, D.; Trcera, N. Investigation of the discoloration of smalt pigment in historic paintings by micro-X-ray absorption spectroscopy at the Co K-edge. *Anal. Chem.* **2011**, *83*, 5145–5152. [CrossRef]
43. Spring, M.; Higgitt, C.; Saunders, D. Investigation of pigment-medium processes in oil paint containing degraded smalt. *Natl. Gallery Tech. Bull.* **2005**, *26*, 56–70.
44. Santopadre, P.; Verità, M. A Study of Smalt and its Conservation Problems in Two Sixteenth-Century Wall Paintings in Rome. *Stud. Conserv.* **2006**, *51*, 29. [CrossRef]
45. Eastaugh, N.; Walsh, V.; Chaplin, T.; Siddall, R. *Pigment Compendium. A Dictionary of Historical Pigments*; Butterworth-Heineman: Oxford, UK, 2004.
46. Prakash Kantha, A.; Rajdeo Singh, M. Vibrational spectroscopy and SEM-EDX analysis of wall painted surfaces, Orchha Fort, India. *J. Archaeol. Sci. Rep.* **2019**, *24*, 434–444.
47. Pacheco, F. *El Arte de la Pintura*; Cátedra: Madrid, Spain, 1990.
48. European Environment Agency. Sulphur Dioxide (SO_2): Annual Mean Concentrations in Europe. 2017. Available online: http://www.eea.europa.eu/themes/air/interactive/so2 (accessed on 15 January 2020).
49. Commission Internationale de l'Eclairage. *Colorimetry*; CIE Publication 15–2; CIE Central Bureau: Vienna, Austria, 1986.
50. Commission Internationale de l'Eclairage. *Colorimetry Part 4: CIE 1976 L*a*b* Colour Space*; CIE S014-4/E; CIE Central Bureau: Vienna, Austria, 2007.
51. Mokrzycki, W.; Tatol, M. Color difference DeltaE-A survey. *Mach. Graph. Vis.* **2011**, *20*, 383–411.
52. International Organization for Standardization. *UNE-EN ISO 4288, Geometrical Product Specifications (GPS). Surface Texture: Profile Method, Terms, Definitions and Surface Texture Parameters*; ISO: Geneva, Switzerland, 1999.
53. International Organization for Standardization. *BS EN 828-Adhesives. Wettability. Determination by Measurement of Contact Angle and Surface Free Energy of Solid Surface*; ISO: Geneva, Switzerland, 2013.
54. Stockmann, G.J.; Wolff-Boenisch, D.; Gislason, S.R.; Oelkers, E.H. Do carbonate precipitates affect dissolution kinetics?: 2: Diopside. *Chem. Geol.* **2013**, *337*, 56–66. [CrossRef]
55. Calligaro, T.; Coquinot, Y.; Picho, L.; Pierrat-Bonnefois, G.; Campos, P.H.O.V.; Re, A.; Angelici, D. Characterization of the lapis lazuli from the Egyptian Treasure of Tod and its Alteration using external u-PIXE and u-IBIL. *Nucl. Instrum. Methods Phys. Res. Sect. B Beam Interact. Mater. At.* **2014**, *318*, 139–144. [CrossRef]
56. Daval, D.; Hellmann, R.; Saldi, G.D.; Wirth, R.; Knauss, K.G. Linking nm-scale measurements of the anisotropy of silicate surface reactivity to macroscopic dissolution rate laws: New insights based on diopside. *Geochim. Et Cosmochim. Acta* **2013**, *107*, 121–134. [CrossRef]
57. Edelstein, S. *Food Science. An Ecological Approach*, 2nd ed.; Jones and Bartlett Learning: Burlington, MA, USA, 2013; p. 678.
58. Nodari, L.; Ricciardi, P. Non-invasive identification of paint binders in illuminated manuscripts by ER-FTIR spectroscopy: A systematic study of the influence of different pigments on the binders' characteristic spectral features. *Herit. Sci.* **2019**, *7*, 7. [CrossRef]

59. Mazzeo, R.; Prati, S.; Quaranta, M.; Joseph, E.; Kendix, E.; Galeotti, M. Attenuated total reflection micro FTIR characterization of pigment-binder interaction in reconstructed paint flims. *Anal. Bioanal. Chem.* **2008**, *392*, 65–76. [CrossRef]
60. Wang, Q.; Sanad, W.; Miller, L.M.; Voigt, A.; Klingel, K.; Kandolf, R.; Stangl, K.; Baumann, G. Infrared imaging of compositional changes in inflammatory cardiomyopathy. *Vib. Spectrosc.* **2005**, *38*, 217–222. [CrossRef]
61. Navas, N.; Romero-Pastor, J.; Manzano, E.; Cardell, C. Benefits of applying combined diffuse reflectance FTIR spectroscopy and principal component analysis for the study of blue tempera historical painting. *Anal. Chim. Acta* **2008**, *630*, 141–149. [CrossRef]
62. Pellegrini, D.; Duce, C.; Bonaduce, I.; Biagi, S.; Ghezzi, L.; Colombini, M.P.; Tinè, M.R.; Bramanti, E. Fourier transform infrared spectroscopic study of rabbit glue/inorganic pigments mixtures in fresh and aged reference paint reconstructions. *Microchem. J.* **2016**, *124*, 31–35. [CrossRef]
63. Bruni, S.; Cariati, F.; Casadio, F.; Toniolo, L. Spectrochemical characterization by micro-FTIR spectroscopy of blue pigments in different polychrome works of art. *Vib. Spectrosc.* **1999**, *20*, 15–25. [CrossRef]
64. Banerjee, A.; Häger, T. On some Crystals of "Lapis Lazuli". *Z. Naturforsch.* **1992**, *47*, 1094–1095. [CrossRef]
65. Derrick, M.R.; Stulik, D.; Landry, J.A. *Infrared Spectrosocpy in Conservation Science. Scientific Tools for Conservations*; The Getty Conservation Institute: Los Angeles, CA, USA, 1999; p. 252.
66. La Russa, M.F.; Ruffolo, S.A.; Barone, G.; Crisci, G.M.; Mazzoleni, P.; Pezzino, A. The Use of FTIR and Micro-FTIR Spectroscopy: An Example of Application to Cultural Heritage. *Int. J. Spectrosc.* **2009**. [CrossRef]
67. De la Rie, E.; Michelin, A.; Ngako, M.; Del Federico, E.; Del Grosso, C. Photo-catalytic degradation of binding media of ultramarine blue containing paint layers: A new perspective on the phenomenon of "ultramarine disease" in painting. *Polym. Degrad. Stab.* **2017**, *144*, 43–52. [CrossRef]
68. Patankar, N.A. Mimicking the Lotus Effect: Influence of Double Roughness Structures and Slender Pillars. *Langmuir* **2004**, *20*, 8209. [CrossRef] [PubMed]
69. Feng, L.; Li, S.; Li, Y.; Li, H.; Zhang, L.; Zhai, J.; Song, Y.; Liu, B.; Jiang, L.; Zhu, D. Super-Hydrophobic Surfaces: From Natural to Artificial. *Adv. Mater.* **2002**, *14*, 1857–1860. [CrossRef]
70. Li, S.; Liu, M.; Sun, L. Preparation of acid-resisting ultramarine blue by novel two-step silica coating process. *Ind. Eng. Chem. Res.* **2011**, *50*, 7326–7331. [CrossRef]